

# Selective inhibition of integrin $\alpha v \beta 6$ leads to rapid induction of urinary bladder tumors in cynomolgus macaques

Magali Guffroy,<sup>1</sup> Bruce Trela,<sup>1</sup> Takahito Kambara,<sup>1</sup> Lukasz Stawski,<sup>2</sup> Huidong Chen,<sup>2</sup> Lia Luus,<sup>2</sup> Monica S. Montesinos,<sup>2</sup> Lauren Olson,<sup>1</sup> Yupeng He,<sup>1</sup> Kevin Maisonave,<sup>1</sup> Tracy Carr,<sup>1</sup> Min Lu,<sup>2</sup> Adrian S. Ray ,<sup>2</sup> Lisa A. Hazelwood<sup>1,\*</sup>

<sup>1</sup>AbbVie, Inc, North Chicago, Illinois 60064, USA

<sup>2</sup>Morphic Therapeutic, Inc, Waltham, Massachusetts 02451, USA

\*To whom correspondence should be addressed at AbbVie, Inc, 1 North Waukegan Rd., North Chicago, IL 60064, USA. E-mail: [lisa.hazelwood@abbvie.com](mailto:lisa.hazelwood@abbvie.com).

Magali Guffroy and Bruce Trela are co-first authorship.

## Abstract

Administration of a novel and selective small molecule integrin  $\alpha v \beta 6$  inhibitor, MORF-627, to young cynomolgus monkeys for 28 days resulted in the rapid induction of epithelial proliferative changes in the urinary bladder of 2 animals, in the absence of test agent genotoxicity. Microscopic findings included suburothelial infiltration by irregular nests and/or trabeculae of epithelial cells, variable cytologic atypia, and high mitotic rate, without invasion into the tunica muscularis. Morphologic features and patterns of tumor growth were consistent with a diagnosis of early-stage invasive urothelial carcinoma. Ki67 immunohistochemistry demonstrated diffusely increased epithelial proliferation in the urinary bladder of several monkeys, including those with tumors, and  $\alpha v \beta 6$  was expressed in some epithelial tissues, including urinary bladder, in monkeys and humans. Spontaneous urothelial carcinomas are extremely unusual in young healthy monkeys, suggesting a direct link of the finding to the test agent. Inhibition of integrin  $\alpha v \beta 6$  is intended to locally and selectively block transforming growth factor beta (TGF- $\beta$ ) signaling, which is implicated in epithelial proliferative disorders. Subsequent *in vitro* studies using a panel of integrin  $\alpha v \beta 6$  inhibitors in human bladder epithelial cells replicated the increased urothelial proliferation observed in monkeys and was reversed through exogenous application of TGF- $\beta$ . Moreover, analysis of *in vivo* models of liver and lung fibrosis revealed evidence of epithelial hyperplasia and cell cycle dysregulation in mice treated with integrin  $\alpha v \beta 6$  or TGF- $\beta$  receptor I inhibitors. The cumulative evidence suggests a direct link between integrin  $\alpha v \beta 6$  inhibition and decreased TGF- $\beta$  signaling in the local bladder environment, with implications for epithelial proliferation and carcinogenesis.

**Keywords:** integrin  $\alpha v \beta 6$  inhibitors; TGF- $\beta$  signaling; urothelial carcinoma; bladder tumors; primate

Integrins are heterodimeric membrane proteins composed of  $\alpha$  and  $\beta$  subunits that regulate cellular activity by integrating the extracellular and intracellular environments in a bidirectional manner (Slack *et al.*, 2022; Springer and Dustin, 2012). Integrins can undergo large conformational changes in response to mechano-biochemical signaling events (Luo and Springer, 2006). There are 3 main states of integrins: a bent closed form, an extended form, and an extended open form. This conformational equilibrium can modulate ligand engagement differing by up to 1000 $\times$  (Li *et al.*, 2021).

Integrins play a central role in the activation of transforming growth factor beta (TGF- $\beta$ ). TGF- $\beta$  isoforms, known as the master regulators of fibrosis, are normally embedded in the extracellular matrix in the latent form before being released by integrin-mediated mechanical force or enzymatic cleavage (Robertson and Rifkin, 2016). The epithelial integrin  $\alpha v \beta 6$  binds to the RGD motif of latency-associated peptide of TGF- $\beta$  as its principal ligand and activates mature TGF- $\beta$ 1 and TGF- $\beta$ 3 to drive fibrogenesis (Shi *et al.*, 2011; Tatler and Jenkins, 2012). ITGB6 (gene encoding the beta subunit of  $\alpha v \beta 6$ ) is expressed in developing tissues

and in a limited number of adult human tissues, including reported low expression in the human urinary bladder epithelium (Breuss *et al.*, 1993, 1995). ITGB6 expression is upregulated in the epithelium of human fibrotic tissues, such as lung epithelium from patients with idiopathic pulmonary fibrosis (IPF) or systemic sclerosis with usual interstitial pneumonitis (Horan *et al.*, 2008); renal tubular epithelium from patients with chronic kidney diseases (Hahm *et al.*, 2007); and biliary epithelium from patients with primary sclerosing cholangitis and primary biliary cirrhosis (Patsenker *et al.*, 2008; Peng *et al.*, 2016; Wang *et al.*, 2007). Similarly, inducible ITGB6 expression has been reported in epithelial cells in rodent models of fibrotic disease (Peng *et al.*, 2016). Because TGF- $\beta$  activation is the rate-limiting step in regulating the bioavailability of TGF- $\beta$ , targeting  $\alpha v \beta 6$  could result in local inhibition of TGF- $\beta$  release, leading to diminished downstream fibroblast activation and production of excess extracellular matrix in tissues. In animal models, inhibition of  $\alpha v \beta 6$  by genetic manipulation or pharmacological inhibition is reported to reduce fibrosis in organs where  $\alpha v \beta 6$  is expressed (Hahm *et al.*, 2007; Peng *et al.*, 2016).

In recent years, several  $\alpha\text{v}\beta\text{6}$  selective inhibitors have been or are being evaluated in clinical trials for fibrosis indications. BG00011 (also known as STX-100, the humanized selective anti- $\alpha\text{v}\beta\text{6}$  antibody 3G9) was the first to initiate a Phase 2B clinical study for IPF but was terminated due to “safety concerns” (Biogen, 2020). GSK3008348, reported as a selective inhaled small molecule  $\alpha\text{v}\beta\text{6}$  inhibitor, was well tolerated in a Phase 1 clinical trial, but further development for IPF was discontinued (GSK, 2019). Oral inhibitors for  $\alpha\text{v}\beta\text{6}$  have also garnered substantial interest as fibrosis treatments. The Phase 1/Phase 2A clinical trial for the less selective molecule IDL-2965, an oral antagonist of  $\alpha\text{v}\beta\text{1}$ ,  $\alpha\text{v}\beta\text{3}$ , and  $\alpha\text{v}\beta\text{6}$  integrins, was terminated due to development challenges and emerging nonclinical data (Indalo, 2019).

MORF-627 is an orally bioavailable, potent, and selective inhibitor of integrin  $\alpha\text{v}\beta\text{6}$  that was a promising development candidate for fibrotic diseases including IPF. In this article, we share the first report of epithelial proliferative changes in the urinary bladder from cynomolgus monkeys administered an  $\alpha\text{v}\beta\text{6}$  inhibitor (MORF-627) in a 28-day Good Laboratory Practice (GLP) oral toxicity study in, and the subsequent studies to elucidate the mechanism of the proliferative findings. From the combined data using studies conducted with different inhibitors of  $\alpha\text{v}\beta\text{6}$  (distinct selectivity and modality, and conformation-independent) coupled with known aspects of broader TGF- $\beta$  signaling, we conclude that the changes observed in bladder were on-target and caused by the interruption of homeostatic regulation of epithelial proliferation by  $\alpha\text{v}\beta\text{6}$ -mediated TGF- $\beta$  activation.

## Materials and methods

### Reagents

MORF-627 is a potent and selective  $\alpha\text{v}\beta\text{6}$  integrin inhibitor (Supplementary Table 1) with good oral bioavailability. This compound is part of the family of integrin inhibitors that stabilize the bent closed conformation of integrins, keeping the receptor in a quiescent state (data not shown). A less selective and structurally distinct tool inhibitor for  $\alpha\text{v}\beta\text{6}$  (example 1 in World Intellectual Property Organization, WO 2017158072) that stabilizes the extended open form of integrins (data not shown), was synthesized by Morphic Therapeutic at ChemPartner and used as a reference control (Supplementary Table 1). An anti- $\alpha\text{v}\beta\text{6}$  antibody (Weinreb et al., 2004) without effector function was generated by Morphic Therapeutic at ATUM Bio, based on the sequence of the variable fragment (Fab) of 3G9 (US patent 8,153,126 B2) fused with the constant fragment (Fc) of mouse IgG1 backbone. Fc-mediated effector function was eliminated by an N297A mutation on the glycosylation site of the Fc region. This effector null 3G9 antibody, which binds to both open and closed conformations, was potent in  $\alpha\text{v}\beta\text{6}$  integrin cell-based assays (0.1–0.2 nM  $\text{IC}_{50}$ ) and used as an on-target control. A small molecule inhibitor, SB-525334 (Peptech Corp), which blocks TGF- $\beta$  receptor type I signaling was used to assess effects of TGF- $\beta$  blockade (Grygielko et al., 2005). The TGF $\beta$ R1/ALK4/JNK3/Flt1 kinase inhibitor previously reported to induce renal epithelial tumors in monkeys (Carreira et al., 2021) was synthesized by AbbVie chemists and used to measure proliferative changes following TGF- $\beta$ R1 inhibition.

### Antibodies and immunohistochemistry

Immunohistochemistry (IHC) was performed on 5  $\mu\text{m}$ -thick, formalin-fixed, paraffin-embedded histological sections from mouse, monkey, or human tissues. All primary antibodies and

pertinent details of the immunohistochemical methods are summarized in Supplementary Table 2.

For mouse tissue IHC, anti-CK19 (clone EP1580Y, 1:1000 dilution, Abcam) and anti-Ki67 (clone SP6, 1:300 dilution, Abcam) antibodies were used as primary antibodies followed by detection and visualization using ImmPRESS Polymer Detection System and ImmPACT NovaRed Peroxidase (HRP) Substrate. The immunostained cells were quantified using a positive stain measurement algorithm.

For monkey and human tissue, chromogen-based IHC stains were performed using automated staining systems, either the BOND Rx Automated Research Stainer (Leica Biosystems, Buffalo Grove, Illinois) or the Ventana Discovery Ultra IHC Stainer (Roche Diagnostics, Indianapolis, Indiana). IHC was performed using the Leica BOND Rx Automated Research Stainer for primary antibodies against the following: Cytokeratin 7 (clone EPR17078, dilution 2.61  $\mu\text{g}/\text{ml}$ , Abcam), Uroplakin III (clone SFI-1, dilution 2  $\mu\text{g}/\text{ml}$ , Abcam), Alpha-smooth muscle actin (clone ACTA2, dilution 0.4  $\mu\text{g}/\text{ml}$ , Abcam), Ki67 (clone MK167, dilution 1  $\mu\text{g}/\text{ml}$ , Invitrogen), and Alpha V beta 6 integrin (clone EM05201, dilution 20  $\mu\text{g}/\text{ml}$ , Absolute Antibody). The Ventana Discovery Ultra IHC Stainer was used for primary antibodies against the following: E-cadherin (clone 36/E-Cadherin, dilution 0.06  $\mu\text{g}/\text{ml}$ , BD Biosciences) and Vimentin (clone V9, dilution 2.5  $\mu\text{g}/\text{ml}$ , Roche Diagnostics). All IHC slides were counterstained with hematoxylin, dehydrated in graded alcohol, cleared with xylene, and coverslipped.

### Probes and in situ hybridization for ITGB6

In situ hybridization (ISH) for ITGB6 (integrin  $\beta\text{6}$ ) was performed on formalin-fixed paraffin-embedded tissue sections with the specific target probes and appropriate positive and negative control probes using the RNAscope 2.5 LS Reagent Kit-BROWN on the Leica Bond Rx automated stainer and the Bond Polymer Refine Detection Kit (DS9800, Leica Biosystems) for color development. The RNA scope assay was run overnight using the manufacturer's recommended protocol (ACD2.5 DAB Rev B with a 2-h hybridization time). ISH probes were purchased from ACDBio (Newark, California) and are detailed in Supplementary Table 3. All ISH slides were counterstained with hematoxylin, dehydrated in graded alcohol, cleared with xylene, and coverslipped.

### Animal husbandry

#### Monkey husbandry

Cynomolgus monkeys (*Macaca fascicularis*) of mainland Asia origin were 2–5 years of age and weighed between 2.7 and 4.3 kg at treatment initiation of the 28-day monkey toxicity study. Monkeys were tested/screened for: SRV, SIV, STLV1, B-virus, Tuberculosis, T cruzi, Measles titer, Salmonella, Shigella, Yersinia, and Campylobacter. In addition, there was fecal testing for ova and parasites. Monkeys were maintained on a 12-h/12-h light/dark cycle with free access to water. Monkeys were offered Certified primate diet twice daily, with the exception of fasting periods required prior to blood collection for the evaluation of clinical pathology parameters.

All procedures performed on animals in the toxicity study were conducted in accordance with established guidelines and regulations and were reviewed and approved by AbbVie's Institutional Animal Care and Use Committee. The Contract Research Organization care facilities that supported this work are fully accredited by the Association for Assessment and Accreditation of Laboratory Animal Care International (AAALAC).

## Mouse husbandry

Male C57BL/6J mice were purchased from The Jackson Laboratory at 7–8 weeks of age. Animals were maintained on a 12-h/12-h light/dark cycle with free access to food and water. All animal procedures were in accordance with Morpnic Therapeutic research guidelines for the care and use of laboratory animals. Both Morpnic and the Contract Research Organization facilities that supported this work are fully accredited by the AAALAC.

## 28-Day oral toxicity study of MORF-627 in cynomolgus monkeys

Monkeys were dosed daily by oral gavage for 4 weeks with vehicle (0.5% HPMC E4M [4000 cps] in Nanopure water [w/v]) or with MORF-627 in vehicle at 30, 60, or 180/120 mg/kg/day ( $N = 3/\text{sex}/\text{group}$ ). The test agent MORF-627 and vehicle control were administered at a dose volume of 5 ml/kg. Initial dosages for this study were based on data obtained from a 2-week dose range-finding toxicity study. Due to clinical signs indicative of intolerability (decreased activity, hunched posture, inappetence, and dehydration) at the high dose of 180 mg/kg/day over the first 3 days of dosing, animals in this dose group were placed on a dosing holiday for approximately 7 weeks from Dosing Day 4, and a full 4-week dosing was then resumed for this dose group at 120 mg/kg/day. The dose level for this group is referred to as 180/120 mg/kg/day.

Blood samples for clinical pathology assessments (hematology, coagulation, and clinical chemistry) were collected from each animal during the baseline phase and twice during the dosing phase (after 1 week of dosing and at necropsy). Urine for urinalysis was collected using clean cage pans over 6–8 h (from the start of the morning light cycle) from each animal during the baseline phase and at the end of the dosing phase. In addition, to standard parameters, urinalysis included microscopic examination of centrifuged sediment for formed elements. Monkeys were euthanized 1 day after the last dosing by intravenous injection of a pentobarbital solution to sedated animals followed by exsanguination. Complete necropsies were performed, and a comprehensive tissue list was collected from each animal and fixed in 10% neutral buffered formalin or other appropriate fixatives. Tissues were processed to paraffin blocks and hematoxylin and eosin-stained sections of all tissues were evaluated and peer reviewed by board-certified veterinary pathologists.

In addition, urinary bladder sections from 2 or 3 animals/group in males and/or females in the control and high-dose groups were immunohistochemically labeled for cytokeratin 7 (CK7), uroplakin III (UPIII), vimentin, alpha-smooth muscle actin ( $\alpha$ -SMA), and E-cadherin, and urinary bladder sections from all study animals were immunolabeled for Ki67.

Quantitative Ki67 analysis was performed on bladder urothelium using a deep learning algorithm developed with Visiopharm version 2020.09 on whole-slide digital images. Urothelium and urothelial nuclei were segmented, and quantification of Ki67-positive nuclei was achieved through thresholding of IHC DAB chromogen intensity. The result was expressed as the number of positive nuclei per 1000 urothelial cells for each sample. The detailed specifications of the developed deep learning models are presented in [Supplementary Table 4](#).

Expression of  $\beta$ 6 protein and/or transcript was evaluated by IHC and/or ISH in monkey urinary bladder (control and high-dose males from 28-day study) and in selected tissues from control monkeys (AbbVie tissue bank) and healthy humans (commercially available tissue microarray).

## Genotoxicity assays

MORF-627 was evaluated by 2 *in vitro* genotoxicity assays at BioReliance Corporation (Rockville, Maryland) in compliance with GLP. The mutagenic potential of MORF-627 was evaluated by measuring induction of reverse mutations at selected loci of several strains of *Salmonella typhimurium* (TA98, TA100, TA1535, and TA1537) and at the tryptophan locus of *Escherichia coli* strain WP2 *uvrA* in the presence and absence of a rat exogenous metabolic activation system. The assay was performed using the preincubation treatment method. In addition, the potential of MORF-627 to induce structural chromosomal aberrations using human peripheral blood lymphocytes (HPBL) was evaluated in both the absence and presence of an exogenous metabolic activation system. HPBL were treated for 4 h in the absence and presence of S9, and for 20 h in the absence of S9. Both assays used dimethyl sulfoxide (DMSO) as the vehicle and included the appropriate positive controls.

## Primary cell culture studies

Normal human bladder epithelial primary cells isolated from the apex, trigone, and neck regions of the bladder were purchased from ATCC (Cat No: PCS-420-010, Donor ID 70036782). The bladder epithelial cells were cultured in serum free bladder epithelial basal medium supplemented with bladder epithelial growth kit from ATCC (Cat No: PCS-420-032 and PCS-420-042, respectively). The bladder cells were cultured from vendor vial and passaged 2 times to expand cell numbers prior to the study. Normal human neonatal alveolar epithelial primary cells as a mixed population of type I and type II cells (AE I/II) were purchased from ScienCell Research Laboratories (Cat No: 3200 Donor 27040). Either bladder or alveolar epithelial cells were seeded in 96-well plates using vendor-recommended media at a density of  $8 \times 10^3$  cells per well. After 24 h, cells were treated with vehicle or tool molecules  $\pm$  TGF- $\beta$ 1 (purchased from Gibco). At each time point, supernatants were removed, and cells were washed and prepared for either RNA expression, flow cytometry, or proliferation assays.

For RNA studies, cells were lysed in 350  $\mu$ l of Buffer RLT containing  $\beta$ -mercaptoethanol ( $\beta$ -ME) prior to RNA isolation (QIAGEN, RNeasy Mini kit). RNA was stored at  $-80^\circ\text{C}$  until endpoints tested. RT-PCR reactions were prepared using template RNA, TaqMan Gene Expression primer probes, and the TaqMan RNA-to-Ct 1-step Master Mix kit (Thermo Scientific). RT-PCR was performed with the Bio-Rad CFX384 Touch system (Bio-Rad) using the cycling program outlined by the manufacturer's protocol. Primer/probes for ITGB6 and housekeeping genes were purchased from Thermo Scientific. ITGB6 expression was calculated via the  $-2\Delta\Delta\text{Ct}$  method using the Vehicle group as control.

For proliferation assays, equal volumes of cell culture medium and Cell Titer Glo 2 reagent (Promega, G9241) were added to the cells. The cells were allowed to lyse for 5 min prior to luminescence measurement on an Envision instrument (PerkinElmer). Graphs were plotted using prism and *p*-value significance was calculated using 2-tailed unpaired *t*-test with Welsh's correction.

## Flow cytometry analysis

Cells were harvested by enzyme-free dissociation (CellStripper, Corning), pelleted (500  $\times$  g, 5 min), and washed once with  $1 \times$  PBS. Then the cells were stained with Zombie UV viability dye (BioLegend) at RT for 15 min. The cells were pelleted and supernatants were removed, followed by incubation with PE mouse-anti-human  $\alpha$ v $\beta$ 6 (clone 10D5, BD #566922, at  $1/200 \times$  dilution in cold BD staining buffer) for 30 min on ice. The cells were

re-pelleted and washed once with cold BD staining buffer. The cells were pelleted once again and resuspended in cold BD staining buffer for flow analysis on a BD Fortessa cell analyzer. Flow cytometry data were analyzed with the FlowJo software. Statistical analysis was performed with GraphPad Prism.

### Mouse fibrosis models

Biliary fibrosis was induced by feeding 8- to 9-week-old mice with a 0.1% DDC (3,5-diethoxycarbonyl-1,4-dihydrocollidine) diet for 21 days (Fickert et al., 2007; Schrier et al., 1983). The small molecule  $\alpha$ v $\beta$ 6 tool inhibitor (10 mg/kg, po, b.i.d.), the TGF $\beta$ R1 inhibitor SB-525334 (30 mg/kg, po, b.i.d.), and the blocking antibody against mouse  $\alpha$ v $\beta$ 6 (3G9; 3 or 10 mg/kg, IP, b.i.w.), were administered in DDC mice starting on day 1 to evaluate their pharmacological effects. Vehicle and mouse IgG1 isotype were used as controls for small molecule and biologic treatments, respectively.

Lung fibrosis was induced by Bleomycin (Hospira USP) via oropharyngeal aspiration at 1.75 U/kg (Munger et al., 1999; Pi et al., 2015). A separate group received saline to serve as the healthy control group. Bleomycin challenged mice were randomized on day 5 based on their percent body weight loss to ensure similar degree of lung injury across all groups. IgG isotype or 3G9 (3 mg/kg, IP, t.i.w.) was administered starting on day 5 for an additional 12 days. On day 17, mice were sacrificed, the post caval lobe was collected for RNA extraction and RNA sequencing, and the remaining lobes were perfusion fixed for histology assessment.

### RNAseq

For RNA-Seq, combined left lateral lobe and right medial lobe from the DDC liver model and mouse post caval lobe from the bleomycin lung model were pulverized, and approximately 30 mg was aliquoted to extract RNA using TRIzol reagent (Life Technologies, Massachusetts) followed by RNeasy Mini Kit (Qiagen). RNA samples with RIN > 7 were selected for sequencing using DNBseq platform (BGI, Hong Kong, China) at a depth of 40 M reads (or 8G Data/sample).

## Results

A potent and selective small molecule antagonist, MORF-627, was identified that stabilized the bent closed conformation of  $\alpha$ v $\beta$ 6 integrin. MORF-627 met the desired properties of a development candidate drug and was found efficacious in bleomycin-induced lung fibrosis model (data not shown). We therefore assessed the safety profile of the compound in cynomolgus monkeys.

### Urothelial carcinoma was observed in the bladder of 2/6 monkeys administered MORF-627 at 180/120 mg/kg/day for 1 month

Monkeys administered MORF-627 at 180 mg/kg/day showed rapidly developing clinical signs of intolerability (mainly decreased activity, hunched posture, inappetence, and dehydration) that led to an extended dosing holiday from Dosing Day 4 with subsequent resuming of dosing at 120 mg/kg/day. There were no MORF-627-related clinical signs or effects on body weight and food consumption at 30, 60, and 120 mg/kg/day. Mean steady-state plasma C<sub>max</sub> levels (total) of MORF-627 on day 28 were 2.6–7.8  $\mu$ M in the 30 and 120 mg/kg/day groups, respectively, and were in excess of the integrin  $\alpha$ v $\beta$ 6 cellular IC<sub>50</sub>.

The observed clinical pathology findings with MORF-627 in this study were limited to the high dose of 180/120 mg/kg/day and included minimal to moderate increases in neutrophil

counts (to 5.6 $\times$  relative to individual baseline) and minimal to mild increases in fibrinogen concentration (to 2.2 $\times$  relative to individual baseline) and C-reactive protein (to 6.3 mg/dl when compared with values  $\leq$ 1.5 mg/dl at baseline). These findings were consistent with an inflammatory response but were not accompanied by correlative microscopic findings. There were no MORF-627-related urinalysis changes at any dose level.

There were no MORF-627-related gross observations or organ weight changes at necropsy at any dose level. MORF-627-related microscopic findings were limited to the urinary bladder, with no observable changes in the urothelium of the renal pelvis. Two of 3 males dosed at 180/120 mg/kg/day had focal poorly circumscribed epithelial tumor masses infiltrating into and expanding the lamina propria of the urinary bladder without invasion into the tunica muscularis (Figs. 1A and 1B). The masses were approximately 2 mm in diameter and were composed of either irregular anastomosing trabeculae (Animal 3003) or variably-sized nests and clusters (Animal 3002) of epithelial cells separated by moderate amounts of slightly mucinous stroma. The trabeculae in Animal 3003 were fairly well organized with orderly architectural appearance, maintenance of cell polarity, and overall minimal nuclear atypia characterized by slight variation in nuclear size with very rare mitotic figures (Figure 1C). The nests and clusters of tumor cells in Animal 3002 displayed disarrayed arrangement of cells, mild nuclear atypia with more frequent mitotic figures, and loss of cell polarity and cohesiveness with scattered single epithelial cells irregularly dispersed and penetrating deep into the lamina propria (Figure 1D). There was pronounced inflammatory cell infiltration within and around the tumors, primarily comprised of eosinophils and lymphocytes with fewer macrophages. The urothelium overlying the tumors was minimally disorganized and/or thickened with microscopic evidence of focal continuity with the subjacent tumors as demonstrated on step sections. The morphologic features and patterns of tumor growth were consistent with a diagnosis of early-stage invasive urothelial carcinoma without vascular invasion or systemic dissemination. In humans, the pattern of invasion has prognostic significance and tumors with infiltrating small clusters and single cells have been shown to have a more aggressive course (Cheng et al., 2012).

The tumor phenotype was further characterized with a panel of immunohistochemical markers. The tumor cells in both animals were strongly positive for cytokeratin 7 (CK7, Figure 2A), whereas they were negative for uroplakin III (UPIII, Figure 2B), vimentin (Figure 2F), and alpha-smooth muscle actin ( $\alpha$ -SMA, Figure 2E). In addition, there was only minimal loss of E-cadherin staining at the leading edge of the tumor mass in Animal 3002 (Figure 2D).

CK7 is expressed in many epithelia, including the epithelium of the urinary bladder. CK7 IHC demonstrated strong and diffuse CK7 expression in both normal urothelium and tumor cells, which enabled unequivocal confirmation of the epithelial histogenesis of the tumors and further outlined the pattern of proprial invasion. UPIII IHC confirmed the expected pattern of expression in the normal urothelium, with staining of differentiated cells (including umbrella and superficial cells) and complete absence of staining of less differentiated basal epithelial cells. The lack of expression of UPIII in the urothelial tumors is consistent with tumors originating from basal urothelial cells or loss of expression with malignant transformation (Olsburgh et al., 2003). Although vimentin and  $\alpha$ -SMA are usually not expressed in epithelial tumors, these proteins may be upregulated during tumor development and mesenchymal transformation, accompanied by motility and invasion of tumor cells. IHC for vimentin and

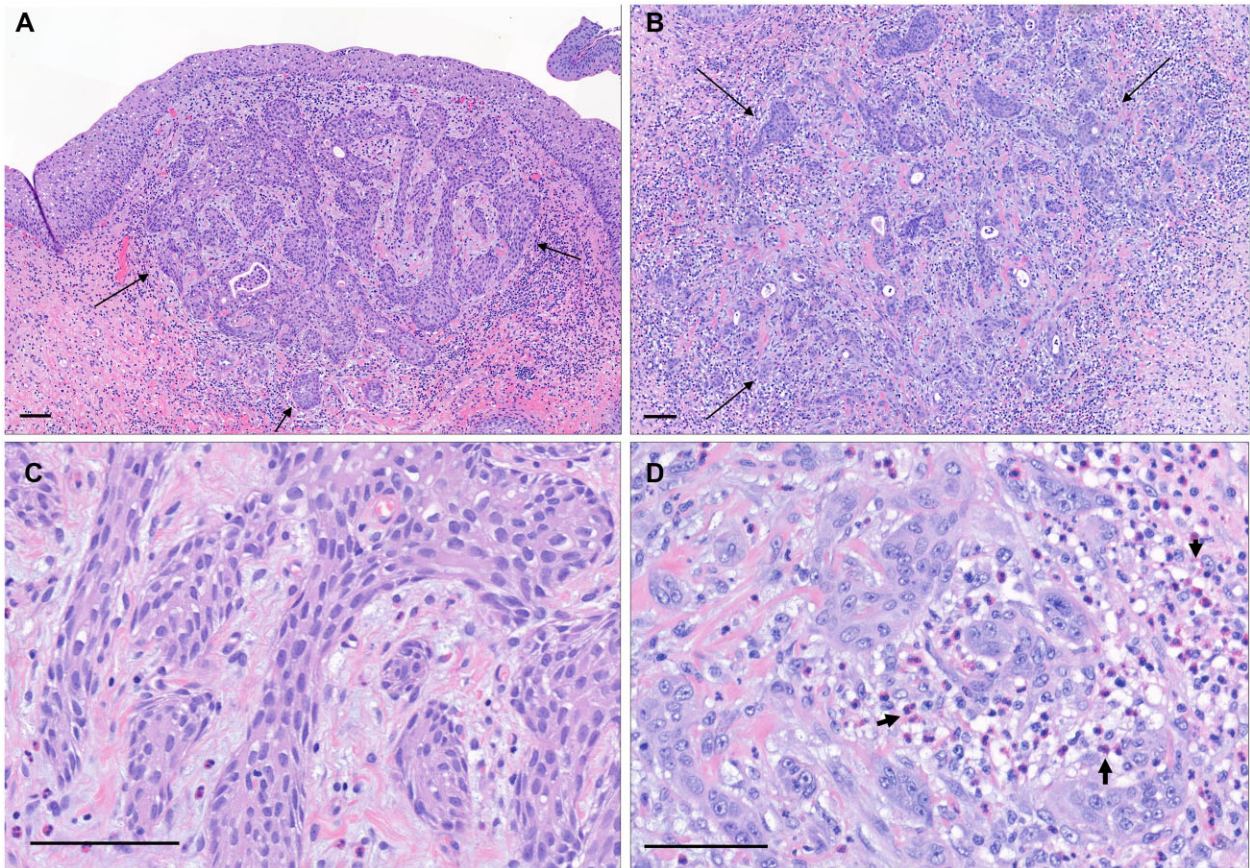


**Figure 1.** Light microscopic features of urinary bladder carcinomas in MORF-627-dosed monkeys. Hematoxylin and eosin stain. Tumor cells are invading into the lamina propria (black arrows) of the urinary bladder in 2 monkeys administered MORF-627 at 180/120 mg/kg/day (A: Monkey 3003; B: Monkey 3002). Higher power magnification showed well-differentiated anastomosing trabeculae with minimal cytonuclear atypia in Animal 3003 (C), whereas there was more disorganized arrangement of tumor cells in Animal 3002 with irregular nests and scattered individual cells displaying loss of polarity, discohesiveness, and moderate nuclear atypia (D). In addition, there was inflammatory cell infiltration in both tumors, that was most prominent in Animal 3002 (D, black arrowheads) and was primarily composed of eosinophils and lymphocytes. Scale bar = 100  $\mu$ m in all panels.

$\alpha$ -SMA confirmed the expected pattern of expression of these proteins in normal bladder tissue but failed to demonstrate expression in tumor epithelial cells. E-cadherin is expressed at adherens junctions in epithelial cells and loss of E-cadherin function may result in a more motile and invasive epithelial cell phenotype with enhanced metastatic potential. There was only minimal loss of E-cadherin membrane expression in small tumor cell clusters at the infiltrating front of the tumor in Animal 3002. Ki67 is a DNA-binding nuclear protein present during all phases of the cell cycle (G1, S, G2, and mitosis) and therefore a marker of cell proliferation. Ki67 IHC of the bladder tumors demonstrated nuclear labeling of many tumor epithelial cells (Figure 2C) in both affected animals accompanied by Ki67 staining of a large number of stromal cells (comprised of both fibroblasts/myofibroblasts and infiltrating inflammatory cells).

Given the critical contribution of cell proliferation to tumor development, Ki67 expression was evaluated in the urinary bladder epithelium of all monkeys from the 28-day toxicity study. Ki67 immunolabeling was very low in all control animals, as expected based on the reported life span of urothelial cells in various species [eg, 40 weeks in adult mice (Jost et al., 1989) and over 200 days in humans (Gaisa et al., 2011)]. The Ki67 score (number of Ki67-positive nuclei per 1000 urothelial cells) varied between 1.0 and 4.8 in the control monkeys from our study. There was significantly increased epithelial cell proliferation (Figure 3)

throughout the urothelium in both monkeys administered MORF-627 at 180/120 mg/kg/day with bladder tumors (Ki67 scores of 48 and 49, respectively) and also in 1 low-dose male and 1 low-dose female monkeys administered MORF-627 at 30 mg/kg/day (Ki67 scores of 55 and 17, respectively). These urinary bladder proliferation data suggest a pathogenetic relationship between increased urothelial proliferation and tumor development.

#### **Integrin subunit $\beta 6$ is expressed in many epithelial tissues, including urinary bladder, in monkeys and humans**

To further explore the contribution of  $\alpha v\beta 6$  integrin target to tumor development, we evaluated the expression of the  $\beta 6$  subunit in monkey and human normal urinary bladder and extended the evaluation to a set of normal tissues in both species. As  $\beta 6$  partners exclusively with  $\alpha v$  to form a single heterodimer, the  $\beta 6$  subunit controls  $\alpha v\beta 6$  expression and availability. We therefore evaluated  $\beta 6$  protein and transcript expression as a surrogate of  $\alpha v\beta 6$  expression.

IHC for  $\beta 6$  subunit demonstrated strong and diffuse, predominantly membrane, staining of urinary bladder epithelium from control monkeys (Figure 4B) and healthy humans (data not shown). The performance of the  $\beta 6$  IHC assay was further confirmed through orthogonal validation using an ITGB6 ISH assay that confirmed the pattern of urinary bladder expression restricted to epithelial cells (Figure 4B, inset). In addition,

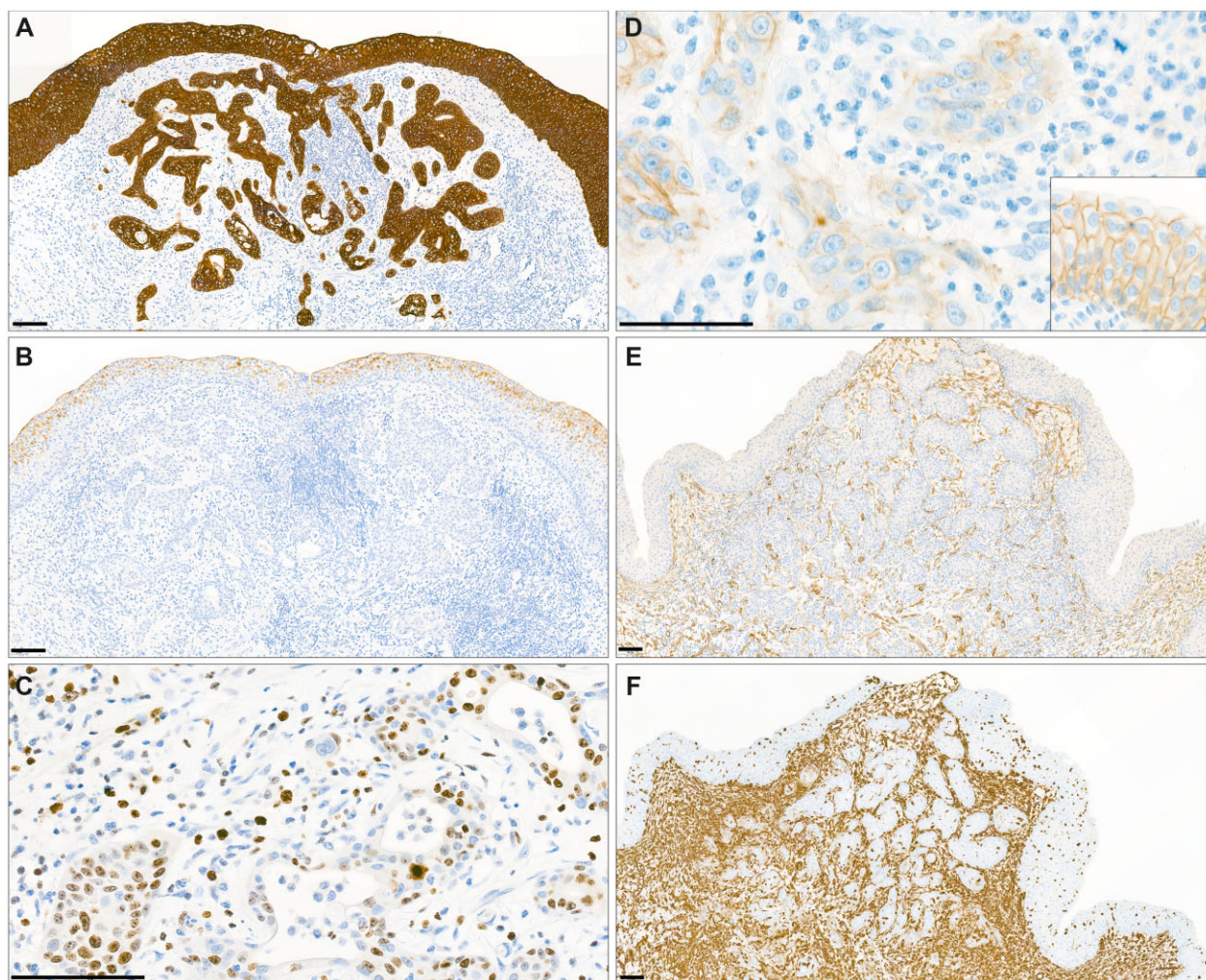


**Figure 2.** Immunohistochemical phenotypic characterization of MORF-627-induced urinary bladder tumors in cynomolgus monkeys. Hematoxylin counterstain. The urinary bladder tumor cells were strongly positive for cytokeratin 7 (A), whereas they were negative for uroplakin III (B), alpha-smooth muscle actin (E), and vimentin (F). In addition, cytokeratin 7 highlighted the pattern of tumor growth and extent of proprial invasion. Ki67 IHC demonstrated an unusually high tumor labeling index with nuclear staining of a large number of tumor epithelial cells (C, black arrows). E-cadherin IHC showed discontinuous and reduced membrane staining in small tumor cell clusters at the leading front of the tumor in one monkey (D) when compared with the level of E-cadherin membrane staining observed in normal bladder urothelium (D, inset). Scale bar = 100  $\mu$ m in all panels.

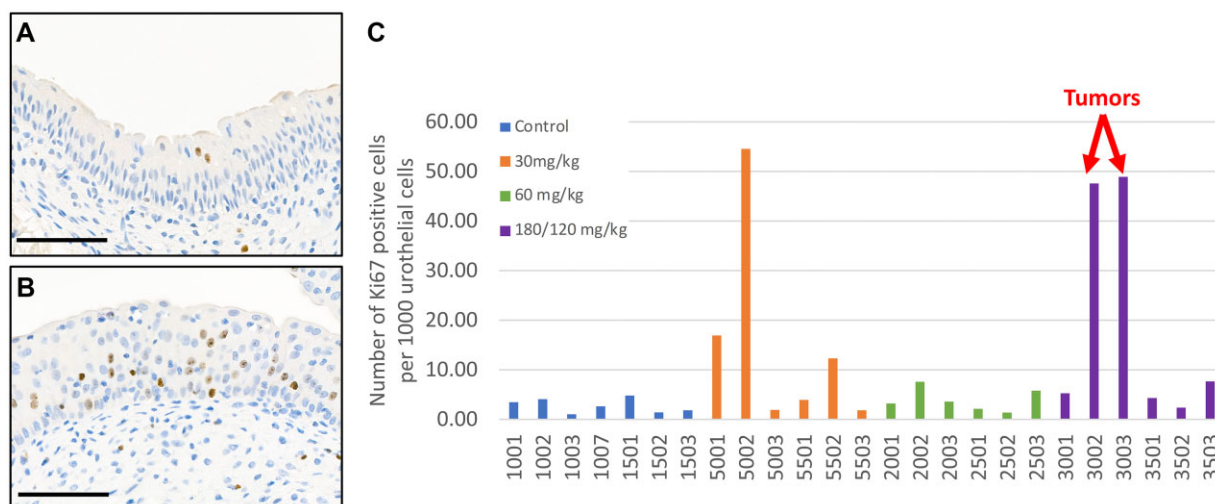


**Figure 3.** Ki67 immunohistochemistry (IHC) in urinary bladder from monkeys dosed with MORF-627 for 28 days. Hematoxylin counterstain. When compared with control animals (A), Ki67 immunohistochemistry demonstrated increased urothelial cell proliferation in the bladder of both monkeys dosed at 180/120 mg/kg/day with bladder tumors (B, C) and also in 2 low-dose monkeys dosed at 30 mg/kg/day (C). Scale bars = 100  $\mu$ m in all panels.

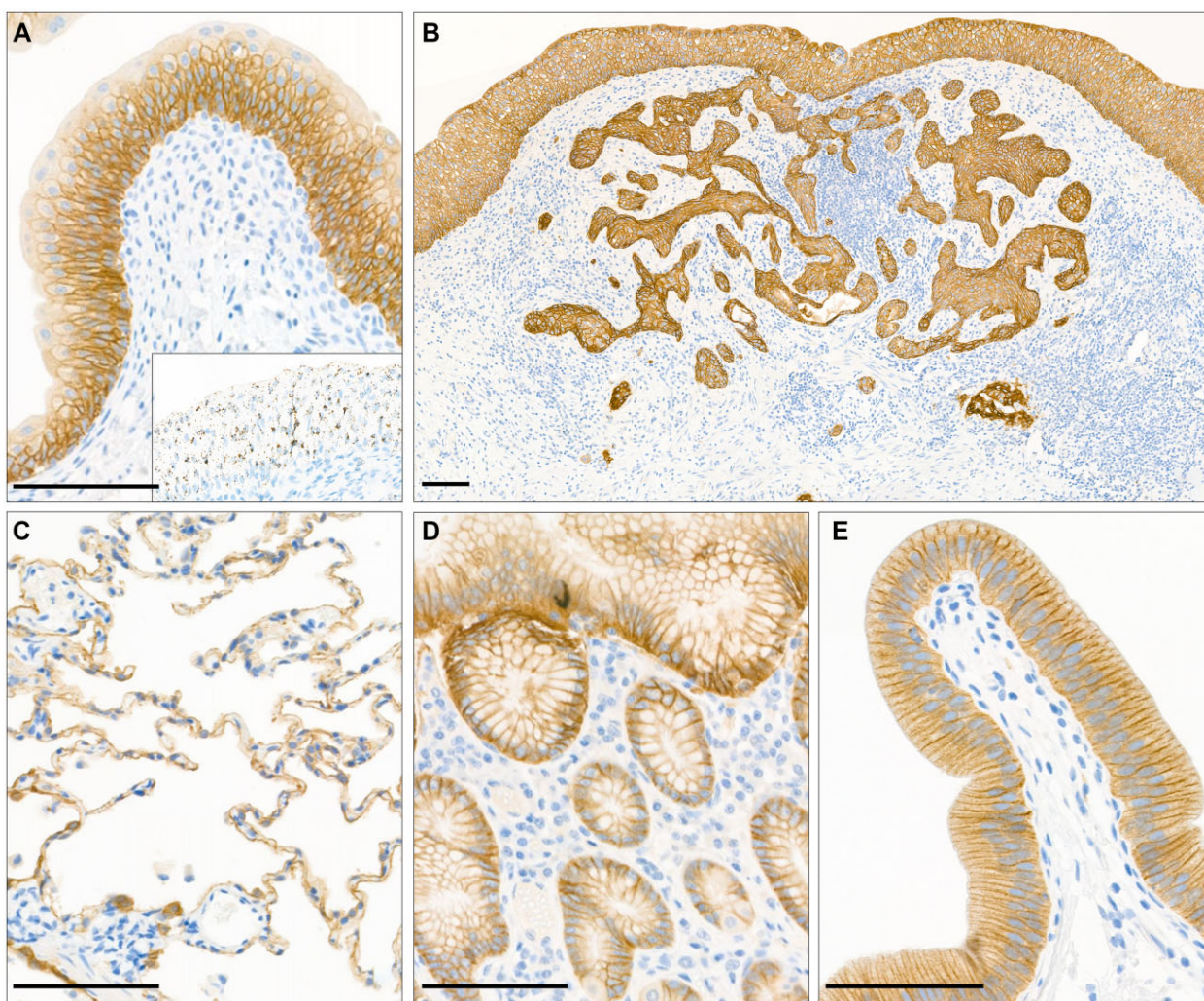


**Figure 4.** Immunohistochemical characterization of  $\beta6$  subunit expression in monkeys in normal tissues and MORF-627-induced urinary bladder tumors. Hematoxylin counterstain.  $\beta6$  protein was highly expressed in the urothelium of the urinary bladder in control monkeys (A) and in MORF-627-induced bladder tumors (B). ISH confirmed ITGB6 transcript expression in normal bladder urothelium (A, inset).  $\beta6$  protein expression was not limited to the urinary bladder and was observed in several other tissues including lung (C), stomach (D), and gallbladder (E). Scale bar = 100  $\mu\text{m}$  in all panels.

evaluation of  $\beta6$  expression in the bladder tumors from monkeys demonstrated similar protein expression levels (Figure 4A), but lower and inconsistent transcript levels (data not shown), in tumor epithelial cells when compared with healthy urothelium.

IHC for  $\beta6$  was also performed on additional selected normal monkey and human tissues and showed  $\beta6$  membranous expression in epithelial cells from many tissues, including in particular GI tract, urinary tract, lung, and endocrine organs in both species (Monkey: Figs. 4C–E; Human: data not shown). Staining in the GI tract was seen in basal epithelial cells of esophagus and superficial/villous and/or crypt/gland epithelial cells of stomach, small intestine, and large intestine. Staining in the kidney was mainly observed in distal tubules, collecting ducts, and pelvic urothelium. As for the lung,  $\beta6$  expression was observed in bronchiolar epithelial cells and/or alveolar epithelial cells. Moderate to strong  $\beta6$  expression was observed in all these tissues in monkey and human.

#### **MORF-627 was non-genotoxic in 2 in vitro genetic toxicology assays**

MORF-627 was not genotoxic. In the Ames assay, no positive mutagenic responses were observed with any of the tester strains

in either the presence or absence of exogenous rat liver metabolic activation system. In the chromosomal aberration assay, neither statistically significant nor concentration-dependent increases in structural or numerical (polyploid or endoreduplicated cells) aberrations were observed at any concentration in treatment groups with and without S9 ( $p > .05$ ; Fisher's exact and Cochran-Armitage tests). For both assays, all positive and vehicle control values were within acceptable ranges, and all criteria for a valid assay were met. Genotoxicity data for MORF-627 are provided in [Supplementary Tables 5 and 6](#).

#### **MORF-627-induced epithelial proliferation in cultured primary human bladder cells, and proliferative changes were sensitive to TGF- $\beta$**

To build upon the proliferative findings within the monkey bladder epithelium, we performed a series of in vitro studies evaluating the impact of  $\alpha\beta6$  inhibition on proliferation using primary human bladder epithelial cells in culture. Incubation of bladder epithelial cells with  $\alpha\beta6$  inhibitors (MORF-627 and a structurally distinct tool inhibitor) or with a multikinase inhibitor known to block TGF- $\beta$  signaling (Carreira et al., 2021) significantly induced proliferation after 3 days (Figs. 5A–C) or 6 days of treatment.

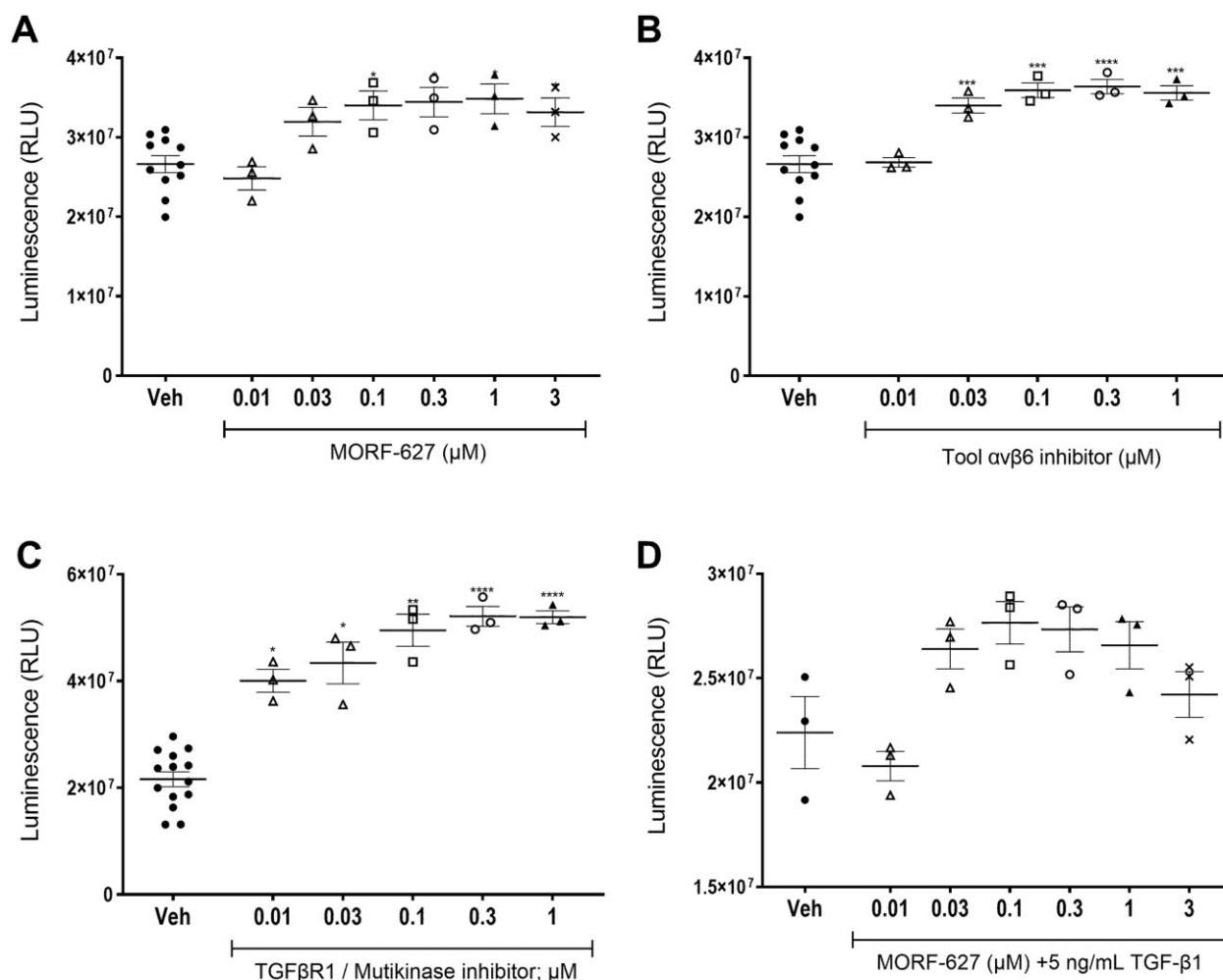


**Figure 5.** Inhibition of  $\alpha v \beta 6$  integrin or TGF $\beta$ R1 induce proliferation in primary human bladder epithelial cells in culture. All proliferation measurements were assessed following 3 days of exposure to treatments. Selective  $\alpha v \beta 6$  integrin inhibitor, MORF-627 (A). Structurally distinct tool  $\alpha v \beta 6$  integrin inhibitor (B). TGF $\beta$ R1 multikinase inhibitor (C). Proliferative changes induced by MORF-627 were reversed by concomitant incubation of test agent with exogenous TGF- $\beta$  (D). Graphs represent 3 independent experiments, with each concentration run in triplicate per study. All data are plotted as raw luminescence mean  $\pm$  SEM; \* $p < .05$ , \*\* $p < .01$ , \*\*\* $p < .001$ , and \*\*\*\* $p < .0001$  indicate statistical significance compared with bleomycin IgG isotype group, using 2-tailed unpaired t-test with Welch's correction.

Treatment with structurally distinct inhibitors of  $\alpha v \beta 6$  or TGF- $\beta$  signaling repressed  $\alpha v \beta 6$  integrin gene (ITGB6, up to 2-fold decrease) and protein ( $\alpha v \beta 6$ , 2.5-fold decrease) expression at 3 days, with a complete rebound in protein expression as measured by flow cytometry after 6 days of treatment (data not shown). These findings mirror the observed changes in the monkey bladder, with increased proliferation, stable  $\beta 6$  protein, and decreased ITGB6 gene expression. To evaluate the role of TGF- $\beta$  signaling in the proliferative changes, we studied the impact of including exogenous TGF- $\beta$  with the MORF-627. Addition of 5 ng/ml exogenous TGF- $\beta$  prevented the proliferative changes observed with compound alone (Figure 5D), increased ITGB6 gene expression, and prevented any change in  $\alpha v \beta 6$  protein expression through day 6 of treatment (data not shown). Loss of primary cell viability over extended duration of culture prevented evaluation of longer time points.

To better understand whether these findings were unique to the bladder epithelium, we also evaluated a second primary human cell type known to express high levels of  $\alpha v \beta 6$ : alveolar epithelial cells. As observed with the bladder epithelial cultures, incubating cells with structurally distinct  $\alpha v \beta 6$  inhibitors or with an inhibitor of TGF- $\beta$ R signaling significantly induced

proliferation 3 and 6 days after treatment (Figs. 6A–C). All compounds decreased ITGB6 gene and  $\alpha v \beta 6$  protein expression. Again, inclusion of exogenous TGF- $\beta$  with MORF-627 reversed the proliferative changes (Figure 6D), and significantly elevated both gene and protein expression across all concentrations of MORF-627 tested.

#### *Inhibition of $\alpha v \beta 6$ integrin confers anti-fibrotic efficacy in mouse models of fibrosis, but also induces epithelial proliferation*

To investigate whether inhibition of  $\alpha v \beta 6$  regulates cell proliferation in other tissue epithelia *in vivo*, we examined liver and lung tissues from mouse models of liver and lung fibrosis where we have evaluated the efficacy of  $\alpha v \beta 6$  inhibition. In the DDC-induced primary sclerosing cholangitis model, expression of  $\alpha v \beta 6$  was significantly elevated in biliary epithelial cells, also known as cholangiocytes (Peng et al., 2016). Treatments with  $\alpha v \beta 6$  inhibitor and a selective TGF $\beta$ R1 inhibitor in the DDC model effectively ameliorated cholestasis and collagen deposition. Unexpectedly, we detected an increase in liver weight in  $\alpha v \beta 6$  and TGF $\beta$ R1 inhibitor-treated mice (data not shown). Despite protection from

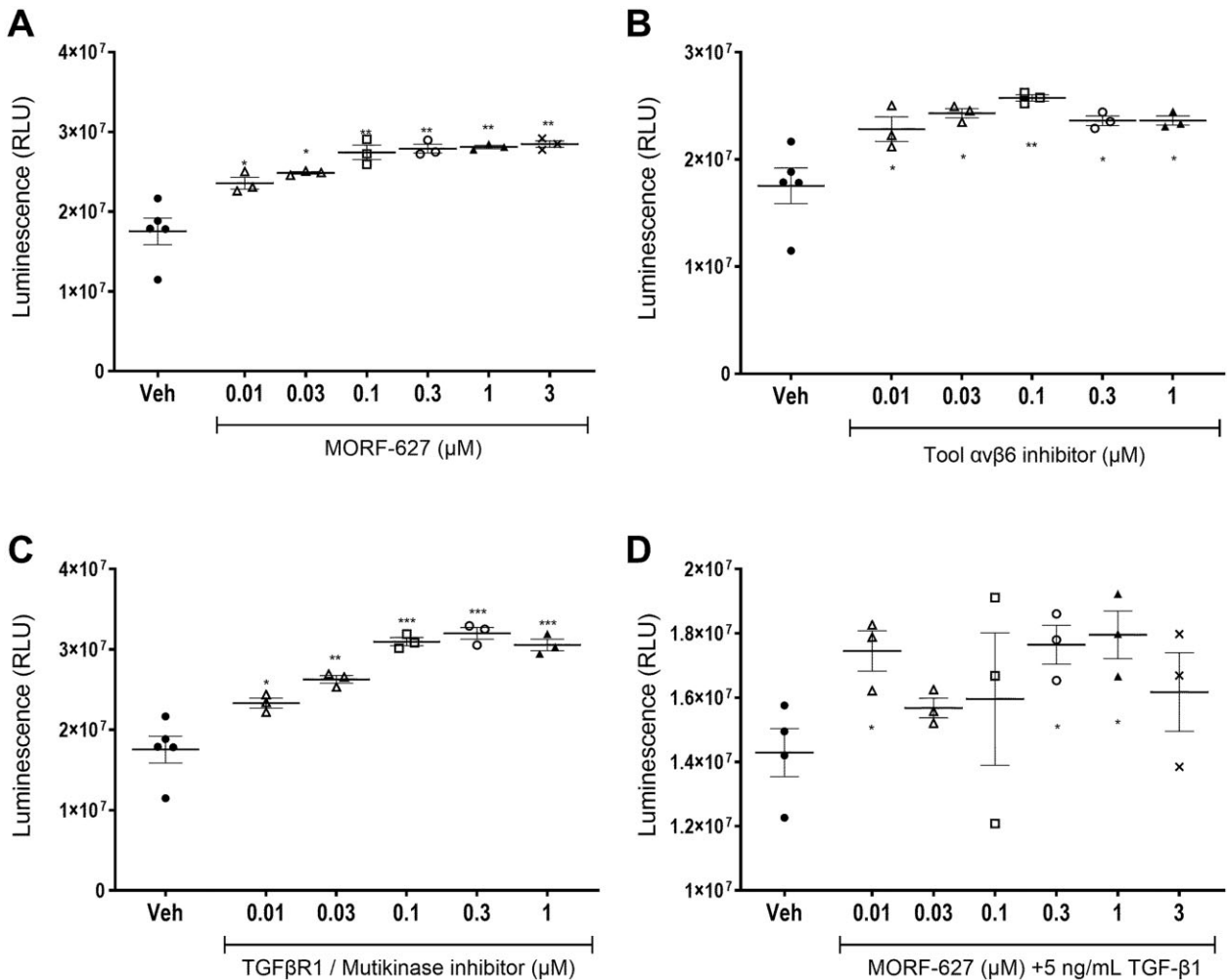


**Figure 6.** Inhibition of  $\alpha v \beta 6$  integrin or TGF $\beta$ 1 induce proliferation in primary human alveolar epithelial cells in culture. All proliferation measurements were assessed following 3 days of exposure to treatments. Selective  $\alpha v \beta 6$  integrin inhibitor, MORF-627 (A). Structurally distinct tool  $\alpha v \beta 6$  integrin inhibitor (B). TGF $\beta$ 1 multikinase inhibitor (C). Proliferative changes induced by MORF-627 were reversed by concomitant incubation of test agent with exogenous TGF- $\beta$  (D). Graphs represent 3 independent experiments, with each concentration run in triplicate per study. All data are plotted as raw luminescence mean  $\pm$  SEM; \* $p < .05$ , \*\* $p < .01$ , \*\*\* $p < .001$ , and \*\*\*\* $p < .0001$  indicate statistical significance compared with bleomycin IgG isotype group, using 2-tailed unpaired t-test with Welch's correction.

fibrosis, there was a paradoxical increase in biliary epithelial cell number as reflected by an increased number of CK19-positive epithelial cells (Figs. 7A and 7B). Similarly, selective blockade of TGF- $\beta$  receptor type I signaling generated comparable results, indicating that the increase in biliary epithelial cells is likely mediated via the  $\alpha v \beta 6$ -TGF- $\beta$  axis. Staining of CK7, another widely used marker for biliary epithelial cells, demonstrated identical patterns of proliferation (data not shown). To investigate whether cellular proliferation caused the increased number of biliary epithelial cells, we measured gene expression of *Mki67* (Ki67) and stained for Ki67 protein. We found that *Mki67* mRNA levels were significantly elevated by both treatments (data not shown). Treatment with the selective TGF $\beta$ 1 inhibitor tripled the number of Ki67-positive cells, and treatment with the tool  $\alpha v \beta 6$  inhibitor increased the number of Ki67-positive cells by nearly 2-fold (Figure 7C). Consistent with findings from small molecule  $\alpha v \beta 6$  inhibitors, DDC mice treated with 3G9, an  $\alpha v \beta 6$  specific antibody whose effector function has been eliminated, demonstrated enlarged livers with less cholestasis (data not shown), and increased numbers of CK19-positive epithelial cells (Figure 8A), despite protection from fibrosis (data not shown).

Administration of 3G9 also led to significantly higher expression of cell cycle and proliferation genes (*Ccnd1*, *Mki67*, and *Pcna*, data not shown) and more Ki67 positive staining (Figure 8B), suggesting target-specific effects of the  $\alpha v \beta 6$  inhibitor on cell proliferation. Lastly, we conducted RNAseq in liver samples from 3G9-treated animals and detected a strong signature in cell cycle regulation (Figure 8C). Taken together, the data suggest that inhibition of  $\alpha v \beta 6$ -dependent TGF- $\beta$  signaling, regardless of treatment modality, enhances biliary epithelial cell proliferation in the DDC mouse model.

To test whether pharmacologic inhibition of  $\alpha v \beta 6$  or TGF- $\beta$  alters lung epithelial cell biology, we administered 3G9 in the bleomycin-induced lung fibrosis model. We observed that 3G9 treatment significantly regulated several gene signatures, including inflammation (Figure 9A), which is consistent with previous publications testing genetic and pharmacological inhibition of  $\alpha v \beta 6$  (Hogmalm et al., 2010; Horan et al., 2008; Puthawala et al., 2008). Pathway analysis for RNAseq data in 3G9 group revealed that DNA replication and cell cycle regulation are among the top pathways modulated by  $\alpha v \beta 6$  inhibition in lung (Figure 9A). There was also a markedly enhanced cell cycle-related gene

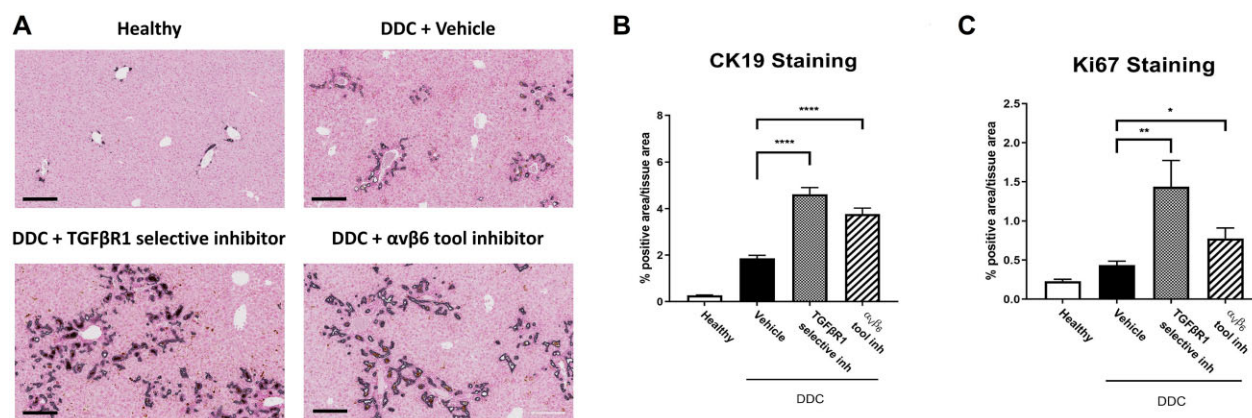


**Figure 7.** Tool  $\alpha v \beta 6$  inhibitor and TGF $\beta$ R1 selective inhibitor increased biliary epithelial cell proliferation in DDC-induced biliary fibrosis model. A, Representative images of IHC staining for CK19 expressing epithelial cells in healthy mice ( $n = 5$ ) and mice fed with DDC diet with or without treatment ( $n = 9-15$ /group). Scale bar = 200  $\mu$ m. B, IHC quantification of CK19 expressing biliary epithelial cells. (\*\*\*\* $p < .0001$  indicate statistical significance compared with DDC vehicle group, using 1-way ANOVA with Dunnett's *post hoc* test.) C, IHC quantification of Ki67 positive proliferating cells (\* $p < .05$ , \*\* $p < .01$  indicate statistical significance compared with DDC vehicle group using 2-tailed Student's T test). All data are shown as means  $\pm$  SEM.

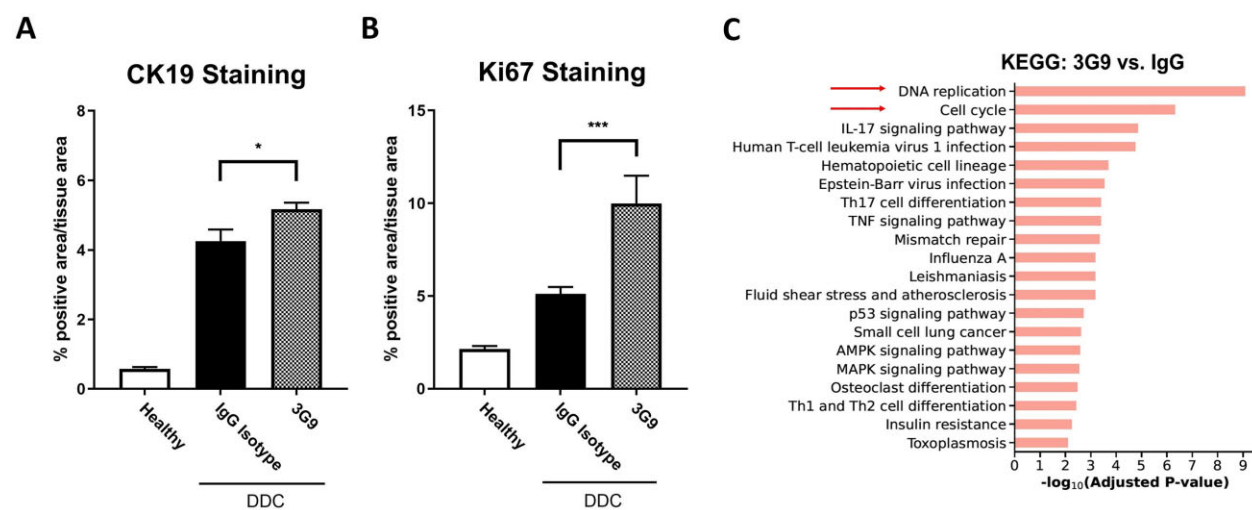


**Figure 8.** Anti- $\alpha v \beta 6$  antibody (3G9) increased biliary epithelial cell proliferation in DDC-induced biliary fibrosis model. A, IHC quantification of CK19 expressing epithelial cells in healthy mice and mice fed with DDC diet with or without treatment ( $n = 10$ /group). B, IHC quantification of Ki67 positive proliferating cells. C, KEGG pathway analysis of bulk RNA sequencing data from liver tissues. All data are shown as means  $\pm$  SEM. \* $p < .05$ , \*\* $p < .01$ , \*\*\* $p < .001$ , and \*\*\*\* $p < .0001$  indicate statistical significance compared with DDC vehicle group, using 1-way ANOVA with Dunnett's *post hoc* test.

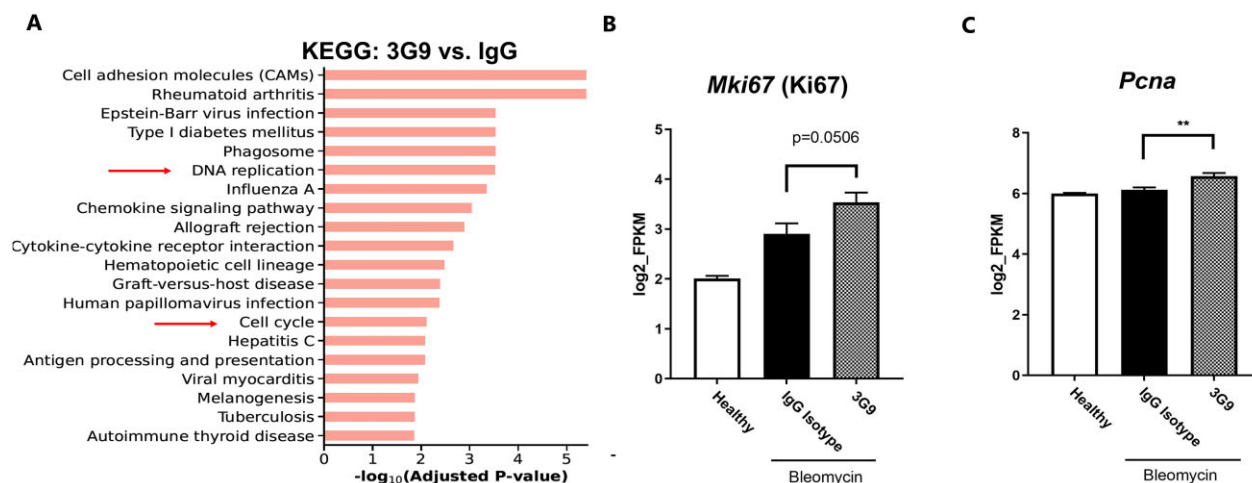


**Figure 9.** Anti- $\alpha v \beta 6$  antibody (3G9) promoted cell proliferation in bleomycin-induced lung fibrosis model. A, KEGG pathway analysis of bulk RNA sequencing data from lung tissues. mRNA levels of cell cycle genes, (B) Mki67 and (C) Pcn $\alpha$ , in lung tissues. All data are shown as means  $\pm$  SEM. \* $p < .05$ , \*\* $p < .01$ , \*\*\* $p < .001$ , and \*\*\*\* $p < .0001$  indicate statistical significance compared with bleomycin IgG isotype group, using 1-way ANOVA with Dunnett's *post hoc* test.

expression profile in the 3G9-treated mice (Figs. 9B and 9C), including increased expression of *Ccnd1* and other cyclin genes (data not shown). Thus, pharmacologic inhibition of the  $\alpha$ v $\beta$ 6/TGF- $\beta$  axis resulted in elevated cell proliferation in 2 different mouse models.

## Discussion

Invasive urothelial tumors were observed in the urinary bladder of 2/6 monkeys administered MORF-627 by oral gavage at 180/120 mg/kg/day for 28 days. Tumor characteristic features of proapoptotic infiltration by irregular nests and/or trabeculae of epithelial cells, loss of cell polarity, variable cytologic atypia, and/or high proliferation rate, without invasion into the tunica muscularis, were consistent with a diagnosis of early-stage urothelial carcinoma. MORF-627 was determined to be non-genotoxic based on *in vitro* bacterial reverse mutation and chromosomal aberration assays.

Spontaneous urothelial carcinomas of the urinary bladder have very rarely been reported in macaques. The review of historical control data from cynomolgus monkeys of various origins (including mainland Asia) assigned to toxicology studies performed between 2012 and 2020 by different Charles River Laboratories Testing Facilities did not identify a single incidence of urothelial tumor in 949 monkeys ranging in age from 1.1 to 7.1 years, whereas proliferative urinary bladder findings were limited to transitional epithelial hyperplasia in 1 out of 949 monkeys (data not shown). Similarly, published information on incidences and range of spontaneous findings in cynomolgus monkeys used in toxicity studies performed by Charles River Laboratories between 2003 and 2009 did not reveal any case of urothelial tumor out of 570 monkeys aged 12–36 months (Chamanza et al., 2010). In addition, no case of urothelial carcinoma was reported in a recent retrospective review of spontaneous urogenital lesions occurring over a 30-year period in various Old World and New World primates at 2 National Primate Research Centers (Kirejczyk et al., 2021). Single case reports of urothelial carcinoma of the bladder have been reported in a young 2.5-year-old rhesus macaque (Chesney and Allen, 1973) and more recently in a 16-year-old female Japanese macaque that was significantly older than animals used routinely in toxicity studies (Johnson et al., 2021). There were no published case reports of spontaneous bladder carcinomas in cynomolgus monkeys over the last 50 years. Spontaneous urinary bladder neoplasms are therefore not expected in cynomolgus monkeys, particularly in young animals of the standard age range for general toxicity studies. In addition, the rigorously monitored health status of the monkeys in the toxicity study reported in this article did not reveal an underlying viral agent or other infectious etiology that could increase the susceptibility to proliferative lesions. In particular, although parasitic infection by *Schistosoma* spp. may be associated with proliferative epithelial lesions of the urinary bladder in monkeys (Cheever et al., 1976), there has been no documented cases of schistosomiasis in monkeys at Charles River Laboratories over the last 5 years. In conclusion, a diligent review of potential confounding causes conclusively indicated that the urothelial carcinomas observed with MORF-627 were not consistent with incidental findings or an infectious etiology.

Experimentally induced urinary bladder neoplasia has been reported in rodents with different classes of genotoxic compounds, such as aromatic amines and nitrosamines, but has very rarely been documented in macaques. Bladder tumors were observed in rhesus monkeys after daily oral administration of the known carcinogen 2-naphthylamine (aromatic amine formerly

used in the manufacture of dyes), with neoplasia ranging from benign papilloma to invasive carcinoma first seen after 33 months (Conzelman et al., 1969). The most common mechanism for bladder tumor induction in rodents with non-genotoxic compounds involves the formation of urinary calculi with secondary chronic urothelial injury, inflammation, and associated proliferation. The bladder tumors induced by MORF-627 in cynomolgus monkeys were highly unusual given the lack of genotoxicity of the compound, extremely short latency period, and absence of associated chronic bladder mucosal injury with epithelial regeneration.

In addition, there was a noteworthy recent publication on drug-induced renal pelvic tumors (Carreira et al., 2021) with notable similarities to the urinary bladder tumors reported in this manuscript. The renal tumors were seen in young 3- to 6-year-old cynomolgus monkeys after nasogastric administration of 2 different multi-kinase inhibitors (with potent inhibition of TGF $\beta$ R1) for 14–21 days. Tumors in all 3 affected monkeys were observed in the pelvic region of the kidneys, with suburothelial infiltration by nests and cords of neoplastic epithelial cells. Based on immunohistochemical characterization of the renal tumors, Carreira et al. suspected a collecting duct origin as the tumors were positive for cytokeratin 19, but negative for CD13 and uroplakin II. However, the absence of uroplakin II expression does not exclude a urothelial origin as uroplakin II is a marker of cell differentiation that may be lost following malignant transformation (Olsburgh et al., 2003). The renal pelvis is lined by the same type of stratified specialized epithelium (urothelium, also referred to as transitional epithelium) as the urinary bladder, and the close proximity and continuity of the renal tumors with the overlying pelvic epithelium were strong suggestions of a possible urothelial origin. The similarities in the mechanism of action of the drugs (TGF $\beta$ R1 inhibition), tumor site (suburothelial), and very short latency period (less than 1 month) suggest a common pathogenesis and an on-target effect for these induced renal and urinary bladder tumors.

To further explore the suspected contribution of  $\alpha$ v $\beta$ 6 inhibition to tumor development,  $\beta$ 6 expression in normal monkey and human tissues was characterized by IHC and/or ISH and demonstrated moderate to strong staining in epithelial cells, not only in the urinary bladder but also in a range of other tissues, including GI tract, urinary tract, lung, and endocrine organs in both species. Therefore, although tumor formation and  $\beta$ 6 expression are coincident, the exceptional urothelial sensitivity to tumor development is not related to a unique pattern of  $\beta$ 6 expression.

In support of the urothelial findings in monkeys, 2 structurally distinct  $\alpha$ v $\beta$ 6 integrin inhibitors produced dose-dependent increases in proliferation in primary human bladder epithelial cells; this finding was further replicated with TGF- $\beta$  receptor inhibition. Notably, the addition of exogenous TGF- $\beta$  to the cell culture environment completely reversed the proliferative phenotype, suggesting an anti-mitotic effect of TGF- $\beta$  on human bladder epithelium. Similar results were observed in primary human alveolar epithelial cells, with induction of proliferation observed following inhibition of  $\alpha$ v $\beta$ 6 integrin, and TGF- $\beta$  enabling reversal of the proliferative changes. In mouse models of liver fibrotic disease,  $\alpha$ v $\beta$ 6 inhibition (small molecule or antibody) or TGF- $\beta$  receptor I blockade resulted in an increase in liver weight, markedly increased number of CK19-positive biliary epithelial cells and Ki67-positive proliferating cells, and augmented expression of cell cycle genes. Dysregulation of cell cycle pathway was also observed in  $\alpha$ v $\beta$ 6 antibody-treated bleomycin lung fibrosis model.

It is noteworthy that our findings extend beyond  $\alpha v\beta 6$  integrin and were replicated with TGF- $\beta$  inhibition. Both *in vitro* and *in vivo*,  $\alpha v\beta 6$ -activated TGF- $\beta$  is crucial for cell cycle regulation, and inhibition of this pathway appears to promote abnormal epithelial cell proliferation. Our studies used different modalities targeting  $\alpha v\beta 6$ /TGF- $\beta$  signaling, including 2 structurally distinct inhibitors of  $\alpha v\beta 6$ , a blocking antibody against  $\alpha v\beta 6$ , and multiple inhibitors of TGF- $\beta$  receptors. These inhibitors were tested in a variety of model systems across 2 human epithelial cell types and 2 mouse models and are in agreement with the epithelial hyperplasia and tumorigenesis observed in  $\alpha v\beta 6$  knockout mice (Ludlow et al., 2005). These results strongly support that abnormal epithelial hyperplasia in the monkey study is mediated by the on-target inhibition of  $\alpha v\beta 6$ -dependent TGF- $\beta$  activation.

The role of  $\alpha v\beta 6$ /TGF- $\beta$  in cell cycle and proliferation is multifaceted. Expression of  $\alpha v\beta 6$  integrin is common in solid tumor cancers and is associated with an adverse prognosis (Desnoyers et al., 2020; Niu and Li, 2017), and some reports suggest that  $\alpha v\beta 6$  may promote cell proliferation *in vitro* and in xenograft models (Dixit et al., 1996; Van Aarsen et al., 2008). TGF- $\beta$  can drive dedifferentiation in epithelial cells via the epithelial-mesenchymal transition process (Kim et al., 2020), which may be necessary for proliferation and tissue repair in the short term. Thus,  $\alpha v\beta 6$  inhibition has been postulated to be useful in the treatment of some cancers. However, it is well established that the roles of TGF- $\beta$  are context dependent, and while it can act as a proliferative factor, it also behaves as an anti-mitogen in many cell types (Zhang et al., 2017). TGF- $\beta$  induces cell cycle arrest at G1 and G2/M, and TGF- $\beta$ /SMAD signaling is considered a tumor suppressive mechanism. Indeed,  $\alpha v\beta 6$  and TGF- $\beta$  were identified as a common tumor suppressor pathway in a genetically engineered mouse model of pancreatic ductal adenocarcinoma (Hezel et al., 2012). Lastly,  $\alpha v\beta 6$  integrin knockout mice displayed epithelial hyperplasia and an increase in both benign and malignant tumors (Ludlow et al., 2005), such as stomach papillomas, squamous cell carcinomas of the ear and stomach, and adenoma and adenocarcinomas of the lungs. Taken together, it appears that  $\alpha v\beta 6$ /TGF- $\beta$  modulation on cell cycle may be context dependent. Whether all  $\alpha v\beta 6$ -expressing epithelial cell types are equally susceptible to the regulation of  $\alpha v\beta 6$ /TGF- $\beta$  axis and whether non- $\alpha v\beta 6$ -expressing cells are influenced by TGF- $\beta$  similarly were not determined in our studies and hence warrant future investigation.

To the best of our knowledge, long-term safety data on  $\alpha v\beta 6$  inhibitor treatment in humans or in carcinogenicity studies in rodents are not available in the general literature. In the repeat-dose mouse studies with 3G9, a low incidence of tumors (such as bronchiolo-alveolar adenoma) was reported to be non-dose-related (Biogen, 2020). The observation of lung adenoma in 3G9-treated mice is reminiscent of similar tumors seen in the knockout mice (Ludlow et al., 2005), although no tumors were noted in monkey studies with 3G9. Similarly, epithelial lesions have been reported in several safety studies and human trials for pan TGF- $\beta$  blockers. As previously noted, renal pelvic tumors and nodular hyperplasia of gallbladder epithelium were observed with short latency periods in cynomolgus macaques treated with 2 small molecule TGF- $\beta$ 1 inhibitors (Carreira et al., 2021; Elmore et al., 2018). Fresolimumab (pan TGF- $\beta$  mAb) showed reversible cutaneous keratoacanthoma/squamous cell carcinoma and hyperkeratosis in phase 1 trial, and there was dose- and time-dependent induction of epithelial hyperplasia of the gingiva and bladder seen in one of the 6-month studies in nonhuman primate (Lonning et al., 2011). Recently, Bintrafusp alfa (a dual PD-L1/TGF-

$\beta$  blocker) was reported to exacerbate recurrent respiratory papillomatosis in humans, compared with PD-L1 antibody alone (Robbins et al., 2021). These adverse findings, including epithelial hyperplasia, papilloma, squamous cell carcinoma, and lung adenoma appear to be consistent with the phenotype of  $\alpha v\beta 6$  knockout mice.

In conclusion, we observed drug-induced proliferative epithelial masses in the urinary bladders of 2 young macaques with very short latency period. The morphologic features and patterns of tumor growth were consistent with a diagnosis of early-stage invasive urothelial carcinoma. These findings were very similar to the recently reported renal pelvic tumors induced by small molecule TGF- $\beta$ 1 inhibitors in monkeys. Although histologic findings in both cases supported a diagnosis of carcinoma, there is currently no experimental data on the behavior of these tumors following treatment cessation, which would contribute to the more definite assessment of the malignant phenotype. Subsequent mechanistic studies of human urinary bladder and lung alveolar epithelial cells, coupled with retrospective analyses from mouse models of disease, strongly implicated the  $\alpha v\beta 6$  integrin/TGF- $\beta$  pathway in the etiology of the tumors. These findings underscore the known breadth of TGF- $\beta$  signaling in cell cycle and carcinogenesis (Carreira et al., 2021; Elmore et al., 2018) and extend the safety concerns with disruption of the TGF- $\beta$  pathway to related mechanisms that indirectly modulate signaling, including but not limited to  $\alpha v\beta 6$  integrin inhibitors.

## Supplementary data

Supplementary data are available at Toxicological Sciences online.

## Acknowledgments

We would like to thank Bryce A. Harrison and James E. Dowling from Morphic Therapeutic for their contributions to the design and chemical synthesis of MORF-627. Morphic Therapeutic received funding from AbbVie as part of a research collaboration agreement. We also thank AbbVie employees Mariana Galindo, Anika Lohse, and Lauren Reinke-Breen for support of primary cell culture studies.

## Funding

AbbVie, Inc.

## Declaration of conflicting interests

M.G., B.T., T.K., L.O., T.C., K.M., Y.H., and L.A.H. are employees of AbbVie. M.L., L.S., M.S.M., and H.C. are employees of Morphic Therapeutic. L.L. and A.S.R. were employees of Morphic Therapeutic at the time of the study. The design, study conduct, and financial support for this research were provided by AbbVie. AbbVie participated in the interpretation of data, writing, review, and approval of the publication.

## References

- Biogen. *An Efficacy and Safety Study of BG00011 in Participants With Idiopathic Pulmonary Fibrosis (Spirit)*. 2020. Available at: <https://clinicaltrials.gov/ct2/show/results/NCT03573505?view=results>.
- Breuss, J. M., Gallo, J., DeLisser, H. M., Klimanskaya, I. V., Folkesson, H. G., Pittet, J. F., Nishimura, S. L., Aldape, K., Landers, D. V., and

- Carpenter, W. (1995). Expression of the beta 6 integrin subunit in development, neoplasia and tissue repair suggests a role in epithelial remodeling. *J. Cell Sci.* **108**, 2241–2251.
- Breuss, J. M., Gillett, N., Lu, L., Sheppard, D., and Pytela, R. (1993). Restricted distribution of integrin beta 6 mRNA in primate epithelial tissues. *J. Histochem. Cytochem.* **41**, 1521–1527.
- Carreira, V., Standeven, A. M., Ma, J. Y., Hardisty, J., Cohen, S. M., Kerns, W. D., and Snook, S. (2021). Inhibitors of TGF $\beta$ 1/ALK4/JNK3/Flt1 kinases in cynomolgus macaques lead to the rapid induction of renal epithelial tumors. *Toxicol. Sci.* **180**, 51–61.
- Chamanza, R., Marxfeld, H. A., Blanco, A. I., Naylor, S. W., and Bradley, A. E. (2010). Incidences and range of spontaneous findings in control cynomolgus monkeys (*Macaca fascicularis*) used in toxicity studies. *Toxicol. Pathol.* **38**, 642–657.
- Cheever, A. W., Kuntz, R. E., Moore, J. A., Bryan, G. T., and Brown, R. R. (1976). Animal model of human disease: Carcinoma of the urinary bladder in schistosoma haematobium infection. *Am. J. Pathol.* **84**, 673–676.
- Cheng, L., MacLennan, G. T., and Lopez-Beltran, A. (2012). Histologic grading of urothelial carcinoma: A reappraisal. *Hum. Pathol.* **43**, 2097–2108.
- Chesney, C. F., and Allen, J. R. (1973). Urinary bladder carcinoma in a rhesus monkey (*Macaca mulatta*): A literature review and case report. *Lab. Anim. Sci.* **23**, 716–719.
- Conzelman, G. M., Jr, Moulton, J. E., Flanders, L. E., 3rd, Springer, K., and Crout, D. W. (1969). Induction of transitional cell carcinomas of the urinary bladder in monkeys fed 2-naphthylamine. *J. Natl. Cancer Inst.* **42**, 825–836.
- Desnoyers, A., Gonzalez, C., Perez-Segura, P., Pandiella, A., Amir, E., and Ocana, A. (2020). Integrin  $\alpha$ v $\beta$ 6 protein expression and prognosis in solid tumors: A meta-analysis. *Mol. Diagn. Ther.* **24**, 143–151.
- Dixit, R. B., Chen, A., Chen, J., and Sheppard, D. (1996). Identification of a sequence within the integrin beta6 subunit cytoplasmic domain that is required to support the specific effect of  $\alpha$ v $\beta$ 6 on proliferation in three-dimensional culture. *J. Biol. Chem.* **271**, 25976–25980.
- Elmore, S. A., Carreira, V., Labriola, C. S., Mahapatra, D., McKeag, S. R., Rinke, M., Shackelford, C., Singh, B., Talley, A., Wallace, S. M., et al. (2018). Proceedings of the 2018 national toxicology program satellite symposium. *Toxicol. Pathol.* **46**, 865–897.
- Fickert, P., Stoger, U., Fuchsichler, A., Moustafa, T., Marschall, H. U., Weiglein, A. H., Tsybrovskyy, O., Jaeschke, H., Zatloukal, K., Denk, H., et al. (2007). A new xenobiotic-induced mouse model of sclerosing cholangitis and biliary fibrosis. *Am. J. Pathol.* **171**, 525–536.
- Gaisa, N. T., Graham, T. A., McDonald, S. A., Canadillas-Lopez, S., Poulosom, R., Heidenreich, A., Jakse, G., Tadrous, P. J., Knuechel, R., and Wright, N. A. (2011). The human urothelium consists of multiple clonal units, each maintained by a stem cell. *J. Pathol.* **225**, 163–171.
- Grygielko, E. T., Martin, W. M., Tweed, C., Thornton, P., Harling, J., Brooks, D. P., and Laping, N. J. (2005). Inhibition of gene markers of fibrosis with a novel inhibitor of transforming growth factor-beta type I receptor kinase in puromycin-induced nephritis. *J. Pharmacol. Exp. Ther.* **313**, 943–951.
- GSK. *Single Doses of GSK3008348 in Idiopathic Pulmonary Fibrosis (IPF) Participants Using Positron Emission Tomography (PET) Imaging*. 2019. Available at: <https://clinicaltrials.gov/ct2/show/NCT03069989>.
- Hahm, K., Lukashev, M. E., Luo, Y., Yang, W. J., Dolinski, B. M., Weinreb, P. H., Simon, K. J., Wang, C., Leone, L., Lobb, D. R., et al. (2007).  $\alpha$ v $\beta$ 6 integrin regulates renal fibrosis and inflammation in Alport mouse. *Am. J. Pathol.* **170**, 110–125.
- Hezel, A. F., Deshpande, V., Zimmerman, S. M., Contino, G., Alagesan, B., O'Dell, M. R., Rivera, L. B., Harper, J., Lonning, S., Brekken, R. A., et al. (2012). TGF- $\beta$  and  $\alpha$ v $\beta$ 6 integrin act in a common pathway to suppress pancreatic cancer progression. *Cancer Res.* **72**, 4840–4845.
- Hogmalm, A., Sheppard, D., Lappalainen, U., and Bry, K. (2010). Beta6 integrin subunit deficiency alleviates lung injury in a mouse model of bronchopulmonary dysplasia. *Am. J. Respir. Cell Mol. Biol.* **43**, 88–98.
- Horan, G. S., Wood, S., Ona, V., Li, D. J., Lukashev, M. E., Weinreb, P. H., Simon, K. J., Hahm, K., Allaire, N. E., Rinaldi, N. J., et al. (2008). Partial inhibition of integrin  $\alpha$ (v) $\beta$ 6 prevents pulmonary fibrosis without exacerbating inflammation. *Am. J. Respir. Crit. Care Med.* **177**, 56–65.
- Indalo. *A Study of Safety & Blood Levels of IDL-2965 in Healthy Subjects and Patients with a Special Type of Pulmonary Fibrosis*. 2019. Available at: <https://clinicaltrials.gov/ct2/show/NCT03949530>.
- Johnson, A. L., Dozier, B. L., and Colgin, L. M. A. (2021). Urothelial carcinoma in the urinary bladder of a Japanese macaque (*Macaca fuscata*). *J. Med. Primatol.* **50**, 141–143.
- Jost, S. P., Gosling, J. A., and Dixon, J. S. (1989). The morphology of normal human bladder urothelium. *J. Anat.* **167**, 103–115.
- Kim, B. N., Ahn, D. H., Kang, N., Yeo, C. D., Kim, Y. K., Lee, K. Y., Kim, T. J., Lee, S. H., Park, M. S., Yim, H. W., et al. (2020). TGF- $\beta$  induced EMT and stemness characteristics are associated with epigenetic regulation in lung cancer. *Sci. Rep.* **10**, 10597.
- Kirejczyk, S., Pinelli, C., Gonzalez, O., Kumar, S., Dick, E., Jr, and Gumber, S. (2021). Urogenital lesions in nonhuman primates at 2 national primate research centers. *Vet. Pathol.* **58**, 147–160.
- Li, J., Yan, J., and Springer, T. A. (2021). Low-affinity integrin states have faster ligand-binding kinetics than the high-affinity state. *Elife* **10**, e73359.
- Lonning, S., Mannick, J., and McPherson, J. M. (2011). Antibody targeting of TGF- $\beta$  in cancer patients. *Curr. Pharm. Biotechnol.* **12**, 2176–2189.
- Ludlow, A., Yee, K. O., Lipman, R., Bronson, R., Weinreb, P., Huang, X., Sheppard, D., and Lawler, J. (2005). Characterization of integrin beta6 and thrombospondin-1 double-null mice. *J. Cell. Mol. Med.* **9**, 421–437.
- Luo, B. H., and Springer, T. A. (2006). Integrin structures and conformational signaling. *Curr. Opin. Cell Biol.* **18**, 579–586.
- Munger, J. S., Huang, X., Kawakatsu, H., Griffiths, M. J., Dalton, S. L., Wu, J., Pittet, J. F., Kaminski, N., Garat, C., Matthay, M. A., et al. (1999). The integrin  $\alpha$ v $\beta$ 6 binds and activates latent TGF  $\beta$ 1: A mechanism for regulating pulmonary inflammation and fibrosis. *Cell* **96**, 319–328.
- Niu, J., and Li, Z. (2017). The roles of integrin  $\alpha$ v $\beta$ 6 in cancer. *Cancer Lett.* **403**, 128–137.
- Olsburgh, J., Harnden, P., Weeks, R., Smith, B., Joyce, A., Hall, G., Poulosom, R., Selby, P., and Southgate, J. (2003). Uroplakin gene expression in normal human tissues and locally advanced bladder cancer. *J. Pathol.* **199**, 41–49.
- Patsenker, E., Popov, Y., Stickel, F., Jonczyk, A., Goodman, S. L., and Schuppan, D. (2008). Inhibition of integrin  $\alpha$ v $\beta$ 6 on cholangiocytes blocks transforming growth factor-beta activation and retards biliary fibrosis progression. *Gastroenterology* **135**, 660–670.
- Peng, Z. W., Ikenaga, N., Liu, S. B., Sverdlov, D. Y., Vaid, K. A., Dixit, R., Weinreb, P. H., Violette, S., Sheppard, D., Schuppan, D., et al. (2016). Integrin  $\alpha$ v $\beta$ 6 critically regulates hepatic progenitor cell function and promotes ductular reaction, fibrosis, and tumorigenesis. *Hepatology* **63**, 217–232.
- Pi, L., Robinson, P. M., Jorgensen, M., Oh, S. H., Brown, A. R., Weinreb, P. H., Trinh, T. L., Yianni, P., Liu, C., Leask, A., et al. (2015).

- Connective tissue growth factor and integrin alphavbeta6: A new pair of regulators critical for ductular reaction and biliary fibrosis in mice. *Hepatology* **61**, 678–691.
- Puthawala, K., Hadjiangelis, N., Jacoby, S. C., Bayongan, E., Zhao, Z., Yang, Z., Devitt, M. L., Horan, G. S., Weinreb, P. H., Lukashev, M. E., et al. (2008). Inhibition of integrin alpha(v)beta6, an activator of latent transforming growth factor-beta, prevents radiation-induced lung fibrosis. *Am. J. Respir. Crit. Care Med.* **177**, 82–90.
- Robbins, Y., Friedman, J., Clavijo, P. E., Sievers, C., Bai, K., Donahue, R. N., Schlom, J., Sinkoe, A., Hinrichs, C. S., Allen, C., et al. (2021). Dual PD-L1 and TGF- $\beta$  blockade in patients with recurrent respiratory papillomatosis. *J. Immunother. Cancer* **9**, e003113.
- Robertson, I. B., and Rifkin, D. B. (2016). Regulation of the bioavailability of TGF-beta and TGF-beta-related proteins. *Cold Spring Harb. Perspect. Biol.* **8**, a021907.
- Schrier, D. J., Kunkel, R. G., and Phan, S. H. (1983). The role of strain variation in murine bleomycin-induced pulmonary fibrosis. *Am. Rev. Respir. Dis.* **127**, 63–66.
- Shi, M., Zhu, J., Wang, R., Chen, X., Mi, L., Walz, T., and Springer, T. A. (2011). Latent TGF-beta structure and activation. *Nature* **474**, 343–349.
- Slack, R. J., Macdonald, S. J. F., Roper, J. A., Jenkins, R. G., and Hatley, R. J. D. (2022). Emerging therapeutic opportunities for integrin inhibitors. *Nat. Rev. Drug Discov.* **21**, 60–78.
- Springer, T. A., and Dustin, M. L. (2012). Integrin inside-out signaling and the immunological synapse. *Curr. Opin. Cell Biol.* **24**, 107–115.
- Tatler, A. L., and Jenkins, G. (2012). TGF-beta activation and lung fibrosis. *Proc. Am. Thorac. Soc.* **9**, 130–136.
- Van Aarsen, L. A., Leone, D. R., Ho, S., Dolinski, B. M., McCoon, P. E., LePage, D. J., Kelly, R., Heaney, G., Rayhorn, P., Reid, C., et al. (2008). Antibody-mediated blockade of integrin alpha v beta 6 inhibits tumor progression in vivo by a transforming growth factor-beta-regulated mechanism. *Cancer Res.* **68**, 561–570.
- Wang, B., Dolinski, B. M., Kikuchi, N., Leone, D. R., Peters, M. G., Weinreb, P. H., Violette, S. M., and Bissell, D. M. (2007). Role of alphavbeta6 integrin in acute biliary fibrosis. *Hepatology* **46**, 1404–1412.
- Weinreb, P. H., Simon, K. J., Rayhorn, P., Yang, W. J., Leone, D. R., Dolinski, B. M., Pearse, B. R., Yokota, Y., Kawakatsu, H., Atakilit, A., et al. (2004). Function-blocking integrin alphavbeta6 monoclonal antibodies: Distinct ligand-mimetic and nonligand-mimetic classes. *J. Biol. Chem.* **279**, 17875–17887.
- Zhang, Y., Alexander, P. B., and Wang, X. F. (2017). TGF-beta family signaling in the control of cell proliferation and survival. *Cold Spring Harb. Perspect. Biol.* **9**, a022145.